IC/94/139

INTERNATIONAL CENTRE FOR THEORETICAL PHYSICS

ROTATIONAL MELTING IN DISPLACIVE QUANTUM PARAELECTRICS

R. Martoňák

and

E. Tosatti

INTERNATIONAL ATOMIC ENERGY AGENCY

UNITED NATIONS EDUCATIONAL, SCIENTIFIC AND CULTURAL ORGANIZATION

MIRAMARE-TRIESTE

IC/94/139

International Atomic Energy Agency
and
United Nations Educational Scientific and Cultural Organization
INTERNATIONAL CENTRE FOR THEORETICAL PHYSICS

ROTATIONAL MELTING IN DISPLACIVE QUANTUM PARAELECTRICS[1]

R. Martoňák and E. Tosatti
International Centre for Theoretical Physics, Trieste, Italy
and
International School for Advanced Studies (S.I.S.S.A.), Trieste, Italy.

ABSTRACT

Displacive quantum paraelectrics are discussed as possible realizations of rotational quantum melting. The phenomenology of $SrTiO_3$ and $KTaO_3$ is discussed in this light. Both old and fresh theoretical work on two-dimensional lattice models for quantum paraelectricity is reviewed.

MIRAMARE - TRIESTE

June 1994

[1]To appear in a Special Issue of *Solid State Communications* on "*Highlights in Condensed Matter Physics and Materials Science*", ed. by E. Burnstein and A. Pinczuk (1994).

I. INTRODUCTION

A. Historical

Quantum paraelectrics are polar crystals where low-temperature ferroelectricity is only incipient, the reason preventing long-range order being quantum fluctuations. Although the term "quantum paraelectric" seems to have been introduced in 1979 by Müller and Burkard [1], the physical concept is older and appears already in the work of Barrett [2] and of Blinc and Hadži [3] in the 50's. In the latter, in particular, the lack of ordering of some hydrogen-bonded nearly ferroelectric crystals was attributed to dynamical tunneling of the protons between two equivalent sites, corresponding to two opposite orientations of the ferroelectric dipole [4]. Theoretically, this situation was modelled by De Gennes [5], with his well-known mapping onto the quantum Ising model in a transverse field $-t$,

$$H = -J \sum_{(ij)} \sigma_i^z \sigma_j^z - t \sum_i \sigma_i^x , \tag{1}$$

where σ_i^x, σ_i^z are Pauli matrices. The second term represents precisely quantum tunneling term between the two valleys. As the inverse tunneling strength J/t decreases, the Ising transition temperature drops, until at a critical value $(J/t)_c$ all long-range order disappears, yielding a quantum paraelectric state at $T = 0$ (see Sec. IV). The very same model was later advocated for the description of quantum effects in displacive perovskite ferroelectrics such as $BaTiO_3$ by Brout, Müller and Thomas [6]. The prototype displacive quantum paraelectrics of this family are $SrTiO_3$ [1] and $KTaO_3$ [7–9]. These are the systems onto which we will focus our attention in the following, although clearly the general concepts are of wider interest. We should stress that this paper is in no way meant to be complete, either as a discussion, or as a review. Rather, we want to bring out for discussion some questions and viewpoints, both old and new, which appear promising for future developments in this area.

B. Perovskite Ferroelectrics: Classical

In a perovskite ABO_3, such as $BaTiO_3$, the ferroelectric transition is caused by a small permanent displacement of the central cation B (here Ti) towards an off-center position relative to the oxygen cage surrounding it [10] (Fig.1). Hence the term "displacive". The B cation off-center displacement breaks the octahedral symmetry of the cell, and gives rise to a net dipole moment proportional to the B cation relative displacement $\vec{d}_i = \vec{R}_i - \vec{R}_i^0$. Dipoles in different cells interact through a variety of mechanisms and orient parallel to each other, giving rise below T_c to a finite vector order parameter, the polarization $\vec{P} \propto \sum_i \vec{d}_i$. In mean-field theory (reasonable only well below and well above T_c) the individual dipoles are not allowed to fluctuate, and vanish strictly in the disordered, paraelectric phase. Dynamics is controlled by a single collective mode, namely a "soft" lattice vibration, which is in this case a TO $k = 0$ phonon mode, where B and O vibrate in antiphase [10].

Close to T_c, the situation is considerably more complicated, because of several reasons. For one thing, there are always secondary order parameters, such as strain, etc., which couple to the polarization $\vec{P}$, generally favoring a slightly first-order transition. Apart from that, there are in this critical regime important nonclassical fluctuations, connected with the existence of pre-formed local dipoles already *above* T_c. These dipoles form coherent domains whose size is the correlation length ξ. Within them, there is ferroelectric order. However, different domains at distances $\gg \xi$ are incoherent. The walls between these domains execute slow thermal meandering, causing the local time-averaged dipole to vanish in an order-disorder fashion. Therefore, using the language of the classic double-well-plus-spring standard model of structural phase transitions [11], further discussed in Sec. III, even a displacive system like a perovskite, is in an order-disorder regime sufficiently close to T_c. This is sometimes called the "central peak" regime from the strong Raman scattering quasi-elastic peak,

attributed to the domain wall fluctuations.

Microscopically, the energetic reasons why the perovskites ABO_3 become ferroelectric are somewhat subtle, as these systems are relatively wide-gap ionic insulators. The simplest clue is perhaps provided by space-filling geometric considerations. When the relative size of the A cation is very large, so that an overall ideal packing is impossible, and in particular the B-O distance is excessive, then it is most likely for the B cation to move off-center, and break symmetry by approaching one or more of the six oxygens. The electronic structure of the B cation with its empty d-orbitals, and the large nonlinear polarizability of oxygen, however, both play an important role. Recent electronic structure calculations have confirmed this viewpoint, largely due to Migoni, Bilz and Bäuerle [12], and have shown that the shorter B - O bond (the "dipole bond") has a stronger covalent character than the longer ones [13–15]. An interesting, although not necessarily alternative viewpoint, attributes off-center displacement to a pseudo-Jahn-Teller effect [16].

C. Quantum Effects

How do quantum effects enter in a perovskite ferroelectric ? Physically, they will become crucial when the distortion magnitude is so small that the classical energy gain becomes comparable with the quantum level splittings. Suppose we start from the classical ferroelectric, and turn on a weak zero-point motion, say, for simplicity only that of the displaced B cation. Since there are six equivalent valleys, i.e. six equivalent oxygens available for the formation of a shorter B - O bond, the basic quantum process will be tunneling of the B cation between one valley and another, as in De Gennes' model (1). The net effect will be to lower the ferroelectric T_c. As quantum fluctuations, proportional to the intra-cell intervalley tunnel splitting, become stronger than the ferroelectric inter-cell interaction, then an "order-disorder"

quantum paraelectric can be stabilized even at $T = 0$.

In the extreme limit where quantum effects are very large, they can suppress the effect of the lateral energy valleys altogether. In this case, the B ion moves as in a single, centered, harmonic-like potential well with well-spaced intra-cell energy levels. A large inter-cell interaction can still bring about ferroelectric long-range order, even though there is now no intra-cell tendency. This extreme quantum limit, sometimes referred to as the "displacive quantum paraelectric", is amenable to a simpler theoretical description, as will be discussed in Sec.III. Reviews of quantum effects in ferroelectrics are given in Refs.[17–19], mostly emphasizing the displacive viewpoint. Here, we shall shift our attention more towards the opposite, tunneling limit.

D. Rotational Quantum Melting

So far, we have cited mostly old work. What is then the reason to go back to quantum ferroelectrics and paraelectrics ? The main motivation comes from the observation, based on a remarkable series of examples: superfluidity and superconductivity, the fractional quantum Hall effect, mixed valence, heavy fermions and Heisenberg resonating valence bonds, that quantum melting seems never to be trivial. Unlike classical melting, there is deep order in the quantum melted ground state. Even though only the first three examples above have so far shown "super" properties, it is clear that any new case is well worth a closer investigation.

Perovskite quantum paraelectrics are a case of "rotational quantum melting". Each B - O dipole bond, once formed by lowering temperature, can take a multiplicity of orientations inside the oxygen cage, and therefore may be seen as a rotor. The cubic field of the crystalline cage leaves angular momentum of the lowest lying states, $L = 0$ and $L = 1$ (call their energies $E_0 = 0, \Delta$, respectively) unquenched. If a

large ferroelectric coupling J between different cells is present, hybridization between different L states of neighbouring cells becomes dominant. In the ensuing ferroelectric ordered state, rotational symmetry is broken and individual angular momenta are quenched. For sufficiently small $J \ll \Delta$, however, it becomes more convenient to disrupt ferroelectric order, and recover again local rotational invariance, as in the $J \to 0$ limit. In this limit, the ground state is just a product of $L = 0$ states in each cell, it is nondegenerate, and has a finite excitation gap Δ. For finite but small J, the gap will decrease, but symmetry will not change, at $T = 0$, until a critical value $(J/\Delta)_c$, where the gap closes, and ferroelectricity sets in. Conversely, starting from the ferroelectric regime and decreasing J, there is rotational quantum melting at $T = 0$ to a quantum paraelectric state when $(J/\Delta)_c$ is reached. A very similar scenario, in XY version, occurs in granular superconductors [20–24], and for an $N = \infty$ vector model [25].

The main questions which naturally arise here concern the precise nature of the quantum paraelectric state, as well as of how one arrives at it by either varying couplings, or by cooling from the high-temperature classical paraelectric state. The case of $SrTiO_3$, and $KTaO_3$, where experimental evidence is copious, will be our focus. In both cases, bond dipoles appear in an extremely abrupt manner, near 40 K. The reasons why these onsets are so sharp are so far unexplained, and so are other spectroscopic anomalies recently observed at low temperatures [26]. Various new physical mechanisms, which may be expected to play a role in the perovskites will be discussed, even though their detailed connection with the observed anomalies is presently still unsettled.

The layout of this paper is as follows. In Section II, we give a brief summary of experimental facts. It is argued that the alternative order-disorder lattice picture must be used at the onset of quantum paraelectricity in the perovskites. In Section III,

we review the standard displacive transition model applicable to a ferroelectric, both classical and quantum. In Section IV, we present the existing quantum lattice theories, essentially only in two dimensions. Finally, Section V is devoted to a brief summary.

II. SOME EXPERIMENTAL FACTS

In this section we have selected, without any attempt at completeness, a small subset of data which seems pertinent to the following four questions: (i) are $SrTiO_3$ and $KTaO_3$ indeed paraelectric at low temperatures for quantum reasons ? (ii) do pre-formed individual B - O bond dipoles exist or not in the quantum paraelectric regime ? (iii) thermal evolution from classical to quantum paraelectric: a broad crossover, or a sharp transition ? (iv) what lattice dynamical properties does one find in the quantum paraelectric state ?

A. Why is Paraelectricity of Quantum Nature ?

The static dielectric constant ϵ_0 of $SrTiO_3$ and $KTaO_3$ increases on cooling, and until $\sim$ 50 K it shows a normal, classical Curie-Weiss tendency to ferroelectric order. The extrapolated ordering temperatures T^* are $\sim$ 35 K [1] and $\sim$ 40 K [7–9], respectively. However, no actual divergence occurs at these temperatures. There is instead a leveling off of ϵ_0, eventually reaching, for $T < 10$ K, extremely high values ($\sim 10^4$). These systems apparently remain stuck close to an incipient, but never-coming critical point roughly from T^* down to $T = 0$.

A number of authors have attributed this incipient ferroelectric behaviour to quantum mechanical suppression of ferroelectricity [17–19,27]. In strong analogy with the hydrogen-bonded systems [28], where quantum effects are well-established, low-temperature long-range order in these perovskites can be turned on and off by uniaxial

and by hydrostatic pressure respectively [7,29–33]. Here, the latter causes an overall bond shortening which reduces the off-center well depth for the B ion, and makes fluctuations, both classical and quantum, more important. Uniaxial pressure, conversely, widens the lattice spacing normal to its direction, and this favors ferroelectric ordering and suppresses fluctuations when dipoles order along that normal direction. Particularly convincing is also the evidence for a quantum paraelectric- ferroelectric phase transition which can be obtained by doping. Examples are $Sr_{1-x}Ba_xTiO_3$ [34], $KTa_{1-x}Nb_xO_3$, $K_{1-x}Na_xTaO_3$ [35], and $Sr_{1-x}Ca_xTiO_3$ [36], where a ferroelectric $T = 0$ transition takes place for very small critical values of x. The weak ferroelectric state obtained in this way exhibits a clear quantum character. The critical temperature T_c approaches zero in the quantum fashion $(p - p_c)^{1/2}$ or $(x - x_c)^{1/2}$ [27]. The specific heat shows no anomalies (corresponding to a negative specific heat exponent α) [19,37] and also a quantum susceptibility exponent $\gamma = 2$ has been argued in this regime [17,19,38]. Isotope effects have also been predicted in mean-field theory [38], but have apparently not been pursued experimentally so far.

There is so far no detailed analysis of the exact origin of the quantum effects. Neither Ti, nor Ta are actually very light nuclei. However, the barrier between different B - O directions inside each cell is small in perovskites, as indicated also by the relative ease with which polarization can be switched from a (100) to a (110) direction. More generally, quantum effects must dominate as soon as the classical would-be order parameter and the corresponding T_c – which can be externally tuned by pressure, etc. – is sufficiently small.

B. Do Local B-O Bond Dipoles Exist at Low Temperatures ?

In a mean-field model of displacive ferroelectricity, the individual B-O bond dipoles exist only in the long-range ordered phase, and disappear together with the or-

der parameter. In an order-disorder system, conversely, the bonds are pre-formed and simply disorder at T_c. What about the displacive quantum ferro and paraelectrics? The available evidence here indicates that B-O bond dipoles are formed at the extrapolated Curie-Weiss temperature T^*, quite suddenly, even if in a thermodynamically gentle manner, apparently without any strong accompanying phenomena, such as lattice strains, entropy change, etc.

A strong evidence for the appearance of B-O bonds at $T^* \simeq 40$ K has been clearly seen by ^{181}Ta NMR in pure $KTaO_3$ [39] (Fig.2), further described in subsection II.C. In $SrTiO_3$, recent Ti K-edge EXAFS data [40] show that the B-O bond length develops large fluctuations near 30 K (Fig.3), which is again close to the extrapolated Curie-Weiss temperature $T^* \simeq 35$ K. Here too, this seems to mark the formation of fluctuating B-O bond dipoles. Additional evidence is provided by spectroscopy. In Raman scattering of $KTaO_3$, nominally cubic down to the lowest temperatures, first order processes are observed [41], contrary to expectations. The existence of small symmetry-broken "ferroelectric microregions", whose size increases from $\sim 2a$ at T^* to $\sim 4a$ at 2 K (a is the lattice parameter) had to be postulated in order to account for the data. A similar conclusion is reached by hyper-Rayleigh scattering in pure $KTaO_3$ [42] and $SrTiO_3$ [43]. A very large hyper-Rayleigh peak builds up below T^*, with intensity growing in the same manner as that of the dielectric constant. It provides evidence of local deviation from cubic symmetry, on time scale longer than 10^{-10} s [42]. Although some undetected defects can, and perhaps should, always be invoked in principle as a nucleation center, the existence of a quasi-static local distortion, and of large, slowly fluctuating domains is generally believed to be a property of the pure host lattice. This also agrees with the finding of very slow dielectric relaxation modes ($\sim$ 100 MHz) which apparently contribute about over 95 % of the static dielectric constant ϵ_0 at 5 K in $KTaO_3$ [44], and are attributed to large fluctuating domains.

We conclude from the above that in the perovskite quantum paraelectrics at and below T^*, the B ion is displaced off-center to form B-O bond dipoles, which fluctuate on a very slow time scale. They are therefore in a quantum order-disorder or "quantum central peak" regime, rather than in a displacive regime.

C. ^{181}Ta NMR in $KTaO_3$ and Fe^{3+} EPR in $SrTiO_3$: A Sharp Transition to the Quantum Paraelectric State ?

Most properties of $KTaO_3$ and $SrTiO_3$ are smooth at the classical paraelectric - quantum paraelectric crossover temperature, $T \sim T^*$, where B-O bond dipoles first appear. A smooth classical - quantum crossover is indeed expected in the simple models, such as the pseudospin model (I), or the extreme quantum displacive limit (see next section). At variance with this picture, however, resonance experiments have demonstrated that the onset of quantum paraelectricity is also accompanied by a sharp anomaly near $T = T^*$.

In ^{181}Ta NMR of pure $KTaO_3$ [39], a sudden inhomogeneous line broadening by a factor ~ 20 appears very close to $T^* \simeq 40$ K on cooling. This indicates that at this temperature most Ta ions suddenly fall into a non-cubic environment on a time scale longer than 10^{-7} s. This kind of transition also takes place in doped samples. It is not apparently accompanied by any global lattice expansion, or dielectric singularity, or other observed thermodynamic feature. Nonetheless it is sharp, reversible and clearly marks the onset of quantum paraelectric regime for $KTaO_3$ (Fig.2).

In $SrTiO_3$, Müller et al. [45] have found evidence by Fe^{3+} EPR of a weak, but sharp phase transition-like anomaly at $T_Q = 37$ K, which again basically coincides with T^*. The data, shown in Fig.4 for negligible and for large (111) pressures, show that the Fe^{3+} impurity magnetic field splittings – sensitive to the local lattice geometry – have a dip, as if a critical phase boundary were crossed at T_Q (Fig.5). There is no

additional level splitting, and thus no apparent lattice symmetry lowering at T_Q, indicating that the transition is not structural. The reduction of the splitting at T_Q suggests a sudden lattice expansion at this temperature. But there is in reality no expansion at all; at T_Q the tetragonal $SrTiO_3$ lattice parameters are totally smooth, and constant, from 50 K down to the lowest temperatures [46]. Also the specific heat of $KTaO_3$ [47] is perfectly smooth and continuous near T^*.

What do these sharp anomalies exactly mean, is at present not understood. While speculation, advanced by Müller et al. [45], that some kind of off-diagonal long-range order (ODLRO) might set in at T_Q is not yet supported by a meaningful order parameter, the coincidence of T_Q with the appearance of B-O bonds, and onset of quantum paraelectricity at T^* is striking. It suggests that the new phase lines of Fig.5 might precisely separate the classical disordered paraelectric state from a quantum rotationally melted state, whose ground state is made of some coherent arrangement of B-O bonds.

D. Anomalous Low-Temperature Dynamical Properties

A number of lattice-dynamical anomalies, appearing simultaneously with quantum paraelectricity, have been found especially in $SrTiO_3$, at temperatures near and below T^*. Already a long time ago, neutron scattering showed in $SrTiO_3$ [48] and in $KTaO_3$ [49] a noticeable coupling between the soft TO_1 mode at $q \simeq 0$ and the TA acoustic branch at $q \simeq \xi^{-1}$, with ξ^{-1} being the inverse correlation length, of about $0.10 \div 0.15(2\pi/a)$ in $KTaO_3$ at 15 K, and $\sim 0.05(2\pi/a)$ in $SrTiO_3$ at 4.5 K. It was pointed out by Axe et al. [49] that, classically, an incommensurate ferroelectricity could arise from such a TO - TA ferroelastic coupling, provided it were strong enough. In reality, there is no incommensurate ferroelectricity (which would be clearly observable), but simply fluctuating ferroelectric microregions, as discussed

in subsection II.B. Due to the ferroelastic coupling, these microregions will also be strain-modulated.

Very recently, much more detailed neutron studies, as well as new Brillouin work have been done on $SrTiO_3$ [26]. Working with monodomain samples, whose c-axis lies along (001), a variety of unexpected anomalies has emerged, in particular: (i) the TO and TA branches are much more complex than it seemed. In particular, for $\vec{q} \parallel (100)$ there are two totally new modes, labeled S and A, respectively (Fig.6), which become substantial only in the quantum paraelectric regime. Since the S-mode frequency is close to that of an E_g mode, forbidden for neutrons in the uniform crystal, it is hypothesized that ferroelectric microdomains induce enough non-uniformity to make it visible. No similar explanation is available for the A-mode. (ii) The intensity of the anomalous acoustic-like branch A propagating in the (a,b) (001) plane (with appreciable polarization along c) weakens rapidly on moving the $\vec{q}$-vector out of the (a,b) plane, and has disappeared already at $\theta \sim 15°$. This is totally unusual, for a phonon mode. (iii) the C_{44} elastic constant softens instead of hardening with decreasing temperature, and the softening is larger in the quantum paraelectric regime. (iv) a new broad peak at finite frequency (a collective excitation ?) appears in Brillouin scattering for $T < T^*$. Finally, additional elastic anomalies in $SrTiO_3$ have been reported by Fossheim et al. [50]. Maxima of the internal friction Q^{-1} and of the elastic compliance S_{11} ($\propto$ inverse sound velocity) have been found, roughly between 20 and 35 K, the latter corresponding closely to T^*, or T_Q. These features are, however, broad, and not sharp as in the case, e.g., of the classical phase transition at 105 K. Their existence seems to be in qualitative agreement with fairly large ferroelectric microdomains of linear size $\xi \sim 10$. Both the onset of decreased sound velocity and the dissipation can probably be attributed to a "dragging" of ferroelectric domain walls by the acoustic wave.

Summarizing this section, there is a fair amount of evidence that well defined individual B-O bond dipoles are formed below T^*, and that these dipoles orient, within ferroelectric microdomains. These domains encompass of the order of ~ 50 ($KTaO_3$) and ~ 1000 ($SrTiO_3$) or more unit cells, and their motion does not appear to freeze out at low temperatures. The onset of quantum paraelectricity is accompanied by unexpectedly sharp signatures in resonance experiments. There are also a number of anomalous dynamical modes, associated with this state, which are not yet understood.

III. CONTINUOUS MODELS

To describe a uniform distortion in a perovskite ABO_3, we need $5 \times 3 = 15$ displacement coordinates (30 in $SrTiO_3$ below 105 K, owing to the antiferrodistortive cell doubling). At finite temperature these coordinates become space and time dependent classical fields. In a quantum paraelectric, they become quantum fields. One is interested in understanding the ground state of such a quantum field theory, and the way it is arrived at as a function of decreasing T. It is clearly of no help, however, to approach the problem at an excessive degree of generality. At the classical level only a small number of displacive order parameters will be important. In a case like $SrTiO_3$, the order parameter is of course the polarization vector $\vec{P}$, mostly related to the Ti displacements, but also the elastic strain tensor $\overleftrightarrow{e}$, and the antiferrodistortive axial vector $\vec{\Phi}$. The latter is missing for cubic $KTaO_3$, which is therefore simpler. In addition, one should consider electric fields and Coulomb forces, connected with the polarization phenomena. In particular, recent work has indicated a very small critical depolarization factor of order 10^{-2} or less for the perovskites [15]. This is probably a reason for the suppression of ferroelectricity in small grains – as observed, for example, by X-rays on powders of $KTa_{1-x}Nb_xO_3$ by Gehring et al. [51]. Sensitivity to depolarizing fields might also severely affect the shape and size of the fluctuating domains in a bulk, and probably deserves a closer investigation. Due to lack of pertinent work, however, we will omit electrostatic effects in the following.

A. Landau - Ginzburg - Wilson Effective Hamiltonian

A Landau-Ginzburg-Wilson effective free energy expansion is a useful phenomenological representation displaying what couplings must be expected from symmetry between the different order parameters. For the case of $SrTiO_3$, several treatments can be found in the literature [52], [53]. Perhaps the most complete and quantitative is that of Uwe and Sakudo [32]. The Helmholtz free energy density f is expanded as a function of polarization $\vec{P}$, cage rotation axial vector $\vec{\Phi}$ and homogeneous lattice strain $\overleftrightarrow{e}$. The symmetry-based expression for the free energy density associated with simultaneous onset of all three uniform order parameters in the otherwise cubic phase is

$$\begin{aligned} f_0(P_l,\phi_l,e_{lk}) - f_0(0) &= \frac{1}{2}\gamma_0 \sum_l P_l^2 + D^x(\sum_l P_l^2)^2 + \frac{1}{2}D_n^x \sum_{l\neq k} P_l^2 P_k^2 \\ &+ \frac{1}{2}\kappa_0 \sum_l \Phi_l^2 + A^x(\sum_l \Phi_l^2)^2 + \frac{1}{2}A_n^x \sum_{l\neq k} \Phi_l^2\Phi_k^2 + \frac{1}{2}\sum_{klmn} c_{klmn}e_{kl}e_{mn} \\ &- \sum_{klmn}\left(g_{klmn}e_{kl}P_mP_n + b_{klmn}e_{kl}\Phi_m\Phi_n + t^x_{klmn}P_kP_l\Phi_m\Phi_n\right), \end{aligned} \tag{2}$$

where most of the constants γ_0, D^x, D_n^x, etc., are given in Ref. [32]. In order to describe space and time fluctuations, this uniform free energy must be supplemented with spatial gradient terms, as well as with a kinetic energy term

$$\begin{aligned} f &= f_{kin} + f_0 + f_{grad} \\ f_{kin} &= \frac{1}{2}m_u \sum_l \dot{u}_l^2(\vec{r}) + \frac{1}{2}m_P \sum_l \dot{P}_l^2(\vec{r}) + \frac{1}{2}m_\Phi \sum_l \dot{\Phi}_l^2(\vec{r}) \\ f_{grad} &= \sum_{klmn} h_{klmn}e_{kl}\frac{\partial P_m}{\partial x_n} + \sum_{klmn} s_{klmn}\frac{\partial P_k}{\partial x_l}\frac{\partial P_m}{\partial x_n} + r(\nabla^2\vec{P})^2 + \sum_{klmn} w_{klmn}\frac{\partial \Phi_k}{\partial x_l}\frac{\partial \Phi_m}{\partial x_n}, \end{aligned} \tag{3}$$

where $\vec{u}(\vec{r})$ is the acoustic displacement field. The $(\nabla\vec{P})^2$, $(\nabla^2\vec{P})^2$ and $(\nabla\vec{\Phi})^2$ terms are obvious. They correspond to a regular dispersion of the pertinent phonon

branches, namely the ferroelectric TO mode branch and the antiferrodistortive TO mode branch (that of the acoustic branch is included in f_0). As for the mixed term, we note that due to the presence of the center of symmetry in the perovskite structure, the effective hamiltonian does not contain the so called Lifshitz invariants, of the type $P_1\nabla P_2 - P_2\nabla P_1$ [54]. We instead have a coupling between the lattice strains and the components of polarization of the form $\sum_{klmn} h_{klmn} e_{kl} \frac{\partial P_m}{\partial x_n}$, which is a generalization of the ferroelastic term adopted in [55]. It gives rise to a $\vec{k}$-dependent coupling between the TO and TA phonon branches (they cannot couple at $\vec{k} \to 0$). A detailed analysis of this classical LGW hamiltonian was performed in [56]. For sufficiently strong coupling h_{klmn} it can give rise to a $\vec{k} \neq 0$ instability resulting in the onset of a spatially modulated, incommensurate phase. The idea of softening of a coupled TO - TA phonon branch leading finally to an onset of INC phase was first advanced by Axe et al [49]. Both $SrTiO_3$ and $KTaO_3$ show some tendency of the TA branch to soften, but no true INC order. Quantum mechanically, one might speculate about the possible existence of the liquid-like "quantum melted INC phase" [56], which could perhaps exist if the quantum kinetic energy were sufficiently strong. However, a detailed study of the full quantum model (3) is presently not available.

B. Standard Single Mode Hamiltonian For Structural Phase Transitions

If one is willing to simplify further, and drop all other order parameters except the polarization, then it is possible to go one step closer to microscopics, by using the standard ("double-well-plus-springs") model of structural phase transitions [11] in its quantum version [27, 57, 58].

After a suitable choice of units for the coordinates and energy, the standard single mode hamiltonian [11] can be written as

$$H = \sum_i \frac{p_i^2}{2M} + \sum_i V(q_i) + \frac{1}{2s}\sum_{\langle ij \rangle}(q_i - q_j)^2 , \tag{4}$$

$$V(q) = -\frac{1}{2}q^2 + \frac{1}{4}q^4 , \tag{5}$$

which consists of a d-dimensional lattice of particles whose continuous displacement is described, for simplicity, by a scalar coordinate q_i. In the quantum case, p_i and q_i become operators satisfying the canonical commutation rules. The model has two parameters, s and M. The value of s, which controls the coupling, also determines whether a displacive or an order-disorder behaviour will prevail in the classical ($M \to \infty$) case: the displacive limit is $s \ll 1$, and the order-disorder limit is $s \gg 1$. The inverse mass M^{-1} measures the strength of the quantum fluctuations. Since we are primarily interested in quantum effects, we have chosen to write the hamiltonian (4) in a form in which the rescaled local potential $V(q)$ (5) has a "normalized double-well" structure. This is useful for identifying the relative importance of quantum effects, which in turn decides when one is in the extreme quantum limit, or in the weak tunneling regime. The two regimes are depicted in Fig.7.

Oppermann and Thomas [57], Schneider, Beck and Stoll [27], and Morf, Schneider and Stoll [59] have considered in detail the quantum ferro-para phase transition of this model at $T = 0$, and have established its new critical exponents, which are different from the classical ones. In particular, the predictions for the specific heat exponent α and the susceptibility exponent γ in d space dimensions are $\alpha = 1 - d, \gamma = 2$, which imply a very weak signature for the ferroelectric phase transition close to quantum $T = 0$ critical point.

C. Microscopic Phonon Modeling: The Oxygen Polarizability

Under the additional assumption that the quantum limit applies, a full microscopic modeling becomes feasible. Bilz and collaborators [38] have built modified

shell models, which embody the nonlinear oxygen polarizability along the B - O bond, and are amenable to a self-consistent harmonic treatment. This type of models accounts well for a number of features of displacive quantum ferroelectrics, including phonon temperature dependence, and quantum freezing phenomena at $T \to 0$. However, there are no pre-formed bonds in this theory and so none of the anomalies observed at and below T^* can be accounted for.

IV. LATTICE MODELS FOR QUANTUM PARAELECTRICS

We did argue in Sec.II, based on a variety of data, that the quantum paraelectric state of perovskites appears to be dominated by order-disorder tunneling fluctuations, in spite of the basic displacive nature of the ferroelectric distortion. In terms of the discussion in Sec.II and III, both $SrTiO_3$ and $KTaO_3$ can be classified as belonging to the tunneling regime at low temperatures. If that were not so, there would be no B - O dipole bonds at low temperatures, where these systems are still paraelectric. Unfortunately, the realistic approaches of Sec.III, based on continuous degrees of freedom, do not work well in the tunneling regime.

As experience with classical systems has shown, strongly fluctuating order-disorder systems are better handled and simulated in a lattice model [60]. When not too damaging for the physical picture, one can further restrict to D=2 space dimensions, which makes reasonably good simulations possible. In this section, we will review and discuss a series of lattice 2D models of quantum para/ferroelectrics in the tunneling regime. The models are ordered so as to include progressively newer and different physical elements inspired by the physics of actual perovskites. One notable point is that in most of these models the B - O bonds are supposed to exist from the start. Therefore, the models can in most cases only be related to the physics of the perovskites at temperatures below T^*. They will not describe immediately e.g., the

sharp NMR broadening transition of $KTaO_3$, and the EPR anomaly of $SrTiO_3$, both of which take place precisely at bond formation. What one may hope to gain, is a better understanding of the low-temperature state.

A. The De Gennes Pseudospin Model

The simplest model is built by considering a double well, with two minima L and R, at each site. A particle sits at each site, it tunnels with hopping amplitude t between L and R, and is linked by a ferro interaction J to the neighbouring sites,

$$H = -t\sum_i (a_i^{L\dagger}a_i^R + a_i^{R\dagger}a_i^L) - J\sum_{\langle ij\rangle}(a_i^{L\dagger}a_i^L a_j^{L\dagger}a_j^L + a_i^{R\dagger}a_i^R a_j^{R\dagger}a_j^R - a_i^{L\dagger}a_i^L a_j^{R\dagger}a_j^R - a_i^{R\dagger}a_i^R a_j^{L\dagger}a_j^L)\,, \tag{6}$$

where $a_i^{L\dagger}a_i^L + a_i^{R\dagger}a_i^R = 1$, and statistics is arbitrary, as there is no propagation. Pseudospin operators can be defined [4]

$$\begin{aligned}\sigma_i^x &= a_i^{L\dagger}a_i^R + a_i^{R\dagger}a_i^L \\ \sigma_i^y &= a_i^{L\dagger}a_i^R - a_i^{R\dagger}a_i^L \\ \sigma_i^z &= a_i^{L\dagger}a_i^L - a_i^{R\dagger}a_i^R\,,\end{aligned} \tag{7}$$

so that H becomes the famous Ising model in a transverse field [5]

$$H = -J\sum_{\langle ij\rangle}\sigma_i^x\sigma_j^x - t\sum_i \sigma_i^z\,, \tag{8}$$

already presented in the Introduction. The behaviour of this model in 2D is very well understood [61–64]. At $T = 0$, there is a quantum para-ferro phase transition at $(J/t)_c \simeq 0.33$, with "quantum" critical exponents [25]. At finite temperature, there is a quantum-classical crossover, such that the actual transition lies inside the classical region, while quantum fluctuations dominate sufficiently far away [65] (Fig.8). As for excitations, both the ferro and the quantum paraelectric state have a gap Δ which

vanishes at the quantum critical point $(J/t)_c$. While for $J > J_c$ there is a ferro-para transition at finite temperatures, there is no phase transition as a function of temperature for $J < J_c$. Here, entropy is activated, in the form $e^{-\Delta/k_B T}$, so that a smooth quantum-classical crossover takes place for $k_B T^* \sim \Delta$.

B. The Quantum Four-State Clock Model

The simplest generalization of the pseudospin model to mimic rotational quantum melting in the perovskites, is to include more than two valleys. Their actual number in $KTaO_3$ is $n = 6$ (equal to the number of oxygens that the central Ta ion can bind). In $SrTiO_3$, the dipoles prefer the (a,b) (001) plane, at least so long as there is an antiferrodistortive order parameter $\vec{\Phi}$ along c. Hence, $n = 4$ in that case. This naturally suggests to consider the $n = 4$ generalization of (8), namely a quantum four-state clock model.

By introducing at each site the clock variable ϕ_i, which can take the four values $0, \pm\pi/2, \pi$, the classical four-state clock model can be written as

$$H^4 = -J \sum_{\langle ij \rangle} \cos(\phi_i - \phi_j) , \tag{9}$$

where we allowed for the interaction between nearest-neighbouring sites.

Classically, the four-state clock model is well understood, as it exactly decouples into two identical Ising models [66]. In fact, representing the clock variable ϕ_i on each site by two auxiliary Ising variables, $\sigma_i, \sigma_i' = \pm 1$, defined respectively by

$$\begin{aligned} \sigma_i &= \sqrt{2} \cos(\phi_i + \frac{\pi}{4}) \\ \sigma_i' &= \sqrt{2} \sin(\phi_i + \frac{\pi}{4}) , \end{aligned} \tag{10}$$

the potential energy term can be immediately written as

$$H^4 = -J \sum_{\langle ij \rangle} \cos(\phi_i - \phi_j) = -\frac{1}{2} J \sum_{\langle ij \rangle} (\sigma_i \sigma_j + \sigma_i' \sigma_j') . \tag{11}$$

The last equation is just Suzuki's classical decoupling [66].

In the quantum case, the clock variable ϕ_i is allowed to hop onto its two nearest orientations, i.e. from ϕ_i into $\phi_i \pm \frac{\pi}{2}$. Describing the system with a wavefunction $\Psi(\phi_1, \ldots, \phi_n)$, the corresponding kinetic piece of hamiltonian operates in the form

$$\begin{aligned} H^{kin\,1} &= \sum_i H_i^{kin\,1} , \\ H_i^{kin\,1} \Psi(\phi_1, \ldots, \phi_i, \ldots, \phi_n) &= -t \left[\Psi(\phi_1, \ldots, \phi_i + \frac{\pi}{2}, \ldots, \phi_n) + \Psi(\phi_1, \ldots, \phi_i - \frac{\pi}{2}, \ldots, \phi_n) \right] . \end{aligned} \tag{12}$$

Interestingly, also the kinetic energy term decouples [67]. In fact, it can be written as

$$\begin{aligned} & H_i^{kin\,1} \Psi(\sigma_1, \sigma_1'; \ldots; \sigma_i, \sigma_i'; \ldots; \sigma_n, \sigma_n') = H_i^{kin\,1} \Psi(\phi_1, \ldots, \phi_i, \ldots, \phi_n) = \\ & -t \left[\Psi(\phi_1, \ldots, \phi_i - \frac{\pi}{2}, \ldots, \phi_n) + \Psi(\phi_1, \ldots, \phi_i + \frac{\pi}{2}, \ldots, \phi_n) \right] = \\ & -t \left[\Psi(\sigma_1, \sigma_1'; \ldots; \sigma_i', -\sigma_i; \ldots; \sigma_n, \sigma_n') + \Psi(\sigma_1, \sigma_1'; \ldots; -\sigma_i', \sigma_i; \ldots; \sigma_n, \sigma_n') \right] . \end{aligned} \tag{13}$$

Because $\sigma_i, \sigma_i' = \pm 1$, we have always $\sigma_i = \pm \sigma_i'$, and the last expression can thus be rewritten as

$$\begin{aligned} & H_i^{kin\,1} \Psi(\sigma_1, \sigma_1'; \ldots; \sigma_i, \sigma_i'; \ldots; \sigma_n, \sigma_n') = \\ & -t \left[\Psi(\sigma_1, \sigma_1'; \ldots; -\sigma_i, \sigma_i'; \ldots; \sigma_n, \sigma_n') + \Psi(\sigma_1, \sigma_1'; \ldots; \sigma_i, -\sigma_i'; \ldots; \sigma_n, \sigma_n') \right] , \end{aligned} \tag{14}$$

in which we recognize the sum of two decoupled tunneling terms. Therefore, the quantum four-state clock model is exactly mapped on the De Gennes model (8).

C. The Constrained Quantum Four-State Clock Model

In a perovskite, the B-O bond formation can be expected to be strongly exclusive of other bonds, engaging either the same B or the same O. In the simple four-state model, the first constraint is always met, the second is not. There will be configurations where two neighbouring clocks point one against the other, which means

two bonds sharing the same oxygen. This configuration is unphysical, and should be projected out. This can be done, for instance, by means of an additional energy U attached to the undesired configurations ($U \to \infty$). For convenience in this and the following subsection, we introduce now a new set of Bose (the choice of statistics will be justified in the next subsection) operators $b_i^{j\dagger}, b_i^j$, with the following meaning. The operator $b_i^{j\dagger}$ creates a state in which there is a dipole bond between the B ion on the site i and the link oxygen O between nearest neighbouring sites i and j, or, in other words, a dipole bond inside the cage i pointing towards cage j. We note that obviously $b_i^{j\dagger} \neq b_j^{i\dagger}$, as the operators refer to different bonds. As there is one and only one bond inside each cage, the operators have to satisfy the constraint $\sum_j b_i^{j\dagger} b_i^j = 1$. The additional U term is then written as

$$H^{constr} = \lim_{U\to\infty} U \sum_{(ij)} b_i^{j\dagger} b_i^j b_j^{i\dagger} b_j^i \,. \tag{15}$$

The term we just introduced is somewhat similar to an ice-type constraint, quite common in the hydrogen-bond ferroelectric models [68]. The constrained model is no longer equivalent to a pseudospin model, and can in principle be expected to exhibit a different critical behaviour, as its Hilbert space is infinitely smaller than the original one [67]. Moreover, the configurations eliminated are ferroelectrically disordered. Thus, one can expect ferroelectric order to be stronger when this constraint is applied. This is precisely what is found by a recent path-integral Monte Carlo study [67], which yields a phase diagram of Fig.9. The quantum critical coupling $(J/t)_c$ in presence of the ice constraint is reduced by more than a factor of four, and the excitation gap is estimated to be smaller by roughly the same factor. However, no new phases have appeared. An activated crossover leads from the classical paraelectric state to the quantum para state, more or less as in the unconstrained model.

D. Bond Hopping, Bond Vacancies

The lightness of oxygen, and its polarizability (the latter implying the possibility to shift electronic charge with great ease and without a large ionic displacement) suggest an additional quantum tunneling process, namely bond hopping. A bond can hop, with hopping matrix element t', from a cell to the next, as for example $B-O\cdots B$ to $B\cdots O-B$, once the middle oxygen tunnels between the two valleys of its effective double well. If large enough, bond hopping could play an important role in the quantum paraelectric state, and, e.g., oxygen isotope studies might ultimately decide whether this process is important or not. Theoretically, it is interesting to note that, if each cell has to have one and only one bond, then bond hopping must by necessity proceed via a closed loop (Fig. 10). This is very reminiscent of collective ring exchange in quantum crystals. Unlike that process, however, circular bond hopping cannot take place inside a well ordered region. It requires a point in the lattice where all four orientations meet. Because of this, only if extremely large, will bond hopping ultimately be effective as a source of quantum disordering at very low temperatures, so long as there is a bond in every cell.

More interesting appears the possible role of bond hopping near the bond dipole formation temperature T^*. Here, one may imagine that a certain number of cells does not possess a bond. Inside these cells, the B ions are still instantaneously centered. Such a "bond vacancy" can be readily filled via bond hopping, i.e. by oxygen tunneling. Now so far, the statistics of the B - O dipole bonds was irrelevant, because they were not allowed to exchange. Having taken into account bond hopping processes, the question of statistics arises. Physically, bonds are composite of (electron pair) + (lattice distortion), and can be thought of as hard-core bosons, the latter statement being true also for the bond vacancies. These bosons are not conserved, however, but will have some lifetime τ_v. Two regimes can then be envisaged, depending on

the relative magnitudes of the vacancy lifetime τ_v and of the bond tunneling time $\tau_h \sim (t')^{-1}$. It is of particular interest to consider the long lifetime limit, $\tau_v \gg \tau_h$, as in this case the vacancies are approximately similar to conserved hard-core bosons on a lattice.

Having allowed for the existence of bond vacancies, the operators $b_i^{j\dagger}$ now have to satisfy the constraint $\sum_j b_i^{j\dagger} b_i^j \leq 1$. In the hamiltonian description, the bond hopping gives rise to an additional piece of kinetic energy, which reads

$$H^{kin\,2} = -t' \sum_{\langle ij \rangle} (b_i^{j\dagger} b_j^i + h.c.) \,. \tag{16}$$

There is an energy cost to create a bond vacancy, equal to the energy barrier V inside the local multiple-well potential for the B ion. This energy plays a role of the negative chemical potential of the bond vacancies. The full hamiltonian of a lattice model with conserved vacancies is

$$H = H^1 + H^{kin\,1} + H^{constr} + H^{kin\,2} + V N_{vac} \,. \tag{17}$$

The $T = 0$ phase diagram of the model is easily determined within the molecular-field approximation [69], and is shown in Fig.11, for the particular case $t' = 3t$. The most interesting feature is the existence of a new broken symmetry non-ferroelectric phase, characterized by the presence of a Bose condensate of bond vacancies, and ODLRO. If such state has to be arrived at by cooling in a real 3D system, it would imply a phase transition at some finite temperature. The transition would obviously be smeared out by vacancy non-conserving processes for finite τ_v.

E. Quadrupolar Interactions, Re-entrance

The simple lattice models discussed so far ignore all other degrees of freedom, particularly lattice strains. One very simple way to include approximately the effect of strain, may be to add a a quadrupolar coupling J_Q, whose presence can be argued

as follows [70]. Suppose a B - O bond dipole $\vec{P}_i$ is formed in a cell i. Due to strain coupling, the cell will become deformed, so as to become longer parallel to $\vec{P}_i$, and correspondingly shorter, orthogonal to $\vec{P}_i$ (Fig. 12). This deformation will carry on to neighbouring cells, where however it will equally favor both states, $\vec{P}_j = \pm \vec{P}_i$, but disfavor the two possibilities at 90°. Therefore the effective strain-induced coupling is quadrupolar (as well as long-ranged), and in the first-neighbour approximation can be written as

$$H^Q = -J_Q \sum_{\langle ij \rangle} \cos 2(\phi_i - \phi_j) \,. \tag{18}$$

Rotational quantum melting in presence of a purely quadrupolar coupling is easily discussed at the mean-field level (see, e.g. [71]), and more accurately so by PIMC [72]. It is realized experimentally by crystalline HD under pressure [73], and is characterized by a *re-entrance* of disorder at low temperatures, which is absent in the purely dipolar case. The mean-field phase diagram [70] of the *quadrupolar* quantum four-state clock model

$$H = H^Q + H^{kin\,1} \tag{19}$$

is shown in Fig.13. The re-entrance is qualitatively similar to that observed in HD. In the past, re-entrance has been argued for the quantum XY model (with dipolar coupling [22]), but has never been convincingly demonstrated. The reason why it appears so readily with quadrupolar couplings can be simply understood at the mean-field level [70], where one treats a rotor in the mean-field of its neighbours. If the gap between the singlet ground state and the (degenerate) first excited state of the rotor decreases as a function of the external field, then the phase boundary between the ordered and the disordered state approaches the $T = 0$ point with a negative slope $\frac{dJ_c}{dJ_Q} < 0$, and the molecular-field phase diagram is reentrant. In case of purely dipolar

interaction, all the rotor eigenstates have a zero dipolar moment, due to inversion symmetry, and therefore in an external field all the eigenvalues become quadratically split. In such a case, it is not obvious whether the gap in an external field will increase or decrease. Apart from the ground state, which is totally symmetric, however, the excited states of a quantum rotor may have a non-zero quadrupolar moment, and therefore may have a linear splitting in an external field. In such case, the gap decreases in an external field and the phase diagram is reentrant.

Studying the joint effect of dipolar and quadrupolar couplings,

$$H = H^Q + H^1 + H^{kin} \,, \tag{20}$$

is the obvious next step. The $T = 0$ phase diagram for this case [70], in the mean field approximation, is shown in the J - J_Q plane in Fig.14. Apart from the disordered (para) phase, it contains both a phase with dipolar order (the ferroelectric order), and one with quadrupolar order, similar to the nematic phase of a liquid crystal. For a ratio J_Q/J larger than 2, we find a finite temperature phase diagram of Fig.15. If we now lower the temperature down along the dashed line, passing close to the reentrant area (Fig.15), we cross a region of enhanced quadrupolar fluctuations without any particular enhancement of the dielectric susceptibility. In principle, it is possible that the EPR experiment on $SrTiO_3$ [45] might have detected precisely this kind of quadrupolar fluctuations.

V. DISCUSSION, AND CONCLUSIONS

We have presented a very qualitative and brief discussion of the quantum paraelectricity in perovskites, particularly $SrTiO_3$ and $KTaO_3$, as an example of rotational quantum melting. Experimentally, slowly fluctuating dipole bonds are present in the low-temperature quantum paraelectric state. Transition from the high-temperature classical paraelectric to the low-temperature quantum paraelectric is at the same

time smooth (dielectric constant, specific heat, elastic properties), and sudden (NMR, EPR), which is intriguing. Neutron and Brillouin spectroscopic studies have brought out a number of interesting low-temperature anomalies. Theoretical modeling is still lagging behind. Realistic models based on continuous degrees of freedom have mostly been applied to the displacive limit, which does not include order-disorder phenomena. Attempts at treating rotational quantum melting for dipole bonds on a lattice are under way, but it is not yet clear when and if they will be able to close the gap between theory and experiment, which is still obviously very large. In particular, the sharp onset of the quantum paraelectric regime remains to be understood in detail, along with most of the lattice-dynamical anomalies. The possible role of defects, which have been ignored in this discussion, also remains to be clarified.

ACKNOWLEDGEMENTS

We wish to acknowledge discussion with, and/or exchange of pertinent information with E. Courtens, P. Fazekas, K. Fossheim, M. Maglione, A. Maritan, D. Marx, K. A. Müller, R. Resta, A. Rigamonti, S. Rod, G. Santoro, S. Sinenoy and S. Sorella. Work at SISSA has been sponsored by INFM and the European Research Office.

REFERENCES

[1] K. A. Müller, H. Burkard, Phys. Rev. B **19**, 3593 (1979).

[2] J. H. Barrett, Phys. Rev. **86**, 118 (1952).

[3] R. Blinc, D. Hadži, Mol. Phys. **1**, 391 (1958).

[4] See, e.g., *Soft Modes in Ferroelectrics and Antiferroelectrics*, R. Blinc and B. Žekš (Elsevier New York 1974).

[5] P. G. de Gennes, Solid State Commun. **1**, 132 (1963).

[6] R. Brout, K. A. Müller and H. Thomas, Solid State Commun. **4**, 507 (1966).

[7] W. R. Abel, Phys. Rev. B **4**, 2696 (1971).

[8] G. A. Samara, B. Morosin, Phys. Rev. B **8**, 1256 (1973).

[9] R. P. Lowndes, A. Rastogi, J. Phys. C **6**, 932 (1973).

[10] *Introduction to Solid State Physics*, C. Kittel (John Wiley & Sons New York 1976).

[11] *Structural Phase Transitions*, A. D. Bruce and R. A. Cowley (Taylor & Francis Ltd. London 1981).

[12] R. Migoni and H. Bilz and D. Bäuerle, Phys. Rev. Lett. **37**, 1155 (1976).

[13] R. E. Cohen, Nature **358**, 136 (1992).

[14] R. D. King-Smith, D. Vanderbilt, Phys. Rev. B **49**, 5828 (1994).

[15] W. Zhong, R. D. King-Smith and D. Vanderbilt, Phys. Rev. Lett. **72**, 3618 (1994).

[16] I. B. Bersuker, Phys. Lett. **20**, 589 (1966); Theor. Expt. Chem. **27**, 227 (1991).

[17] U. T. Höchli, Ferroelectrics **35**, 17 (1981).

[18] K. A. Müller, Jap. J. Appl. Phys., Suppl. **24-2**, 89 (1985).

[19] D. Rytz, Ph.D. thesis N. 475 (1983), Ecole Polytechnique Fédérale de Lausanne.

[20] D. M. Wood and D. Stroud, Phys. Rev. B **25**, 1600 (1982).

[21] K. B. Efetov, Sov. Phys. JETP **51**, 1015 (1980).

[22] E. Šimánek, Phys. Rev. B **23**, 5762 (1980).

[23] P. Fazekas, B. Mühlschlegel, M. Schröter, Z. Phys. B - Condensed Matter **57**, 193 (1984).

[24] C. Bruder, R. Fazio, A. Kampf, A. van Otterlo and G. Schön, Phys. Scr. **42**, 159 (1992).

[25] A. V. Chubukov, S. Sachdev and J. Ye, Phys. Rev. B **49**, 11919 (1994).

[26] E. Courtens, G. Coddens, B. Hennion, B. Hehlen, J. Pelous, R. Vacher, Phys. Scr. **T49B**, 430 (1993).

[27] T. Schneider, H. Beck and E. Stoll, Phys. Rev. B **13**, 1123 (1976).

[28] G. A. Samara and P. S. Peercy, in: *Solid State Physics*, ed. by H. Ehrenreich, F. Seitz, D. Turnbull, Vol. 36 (Academic Prers New York 1981).

[29] G. A. Samara, Ferroelectrics **2**, 177 (1971).

[30] G. Sorge, G. Schmidt, E. Hegenbarth and G. H. Frenzel, Phys. Stat. Sol. **K 37**, 17 (1970).

[31] W. J. Burke and R. J. Presley, Solid State Commun. **9**, 191 (1971).

[32] Hiromoto Uwe and Tunetaro Sakudo, Phys. Rev. B **13**, 271 (1976).

[33] Hiromoto Uwe and Tunetaro Sakudo, Phys. Rev. B **15**, 337 (1977).

[34] H. Gränicher, O. Jakits, Il Nuovo Cimmento Suppl., **11**, 480 (1954).

[35] D. Rytz, U. T. Höchli and H. Bilz, Phys. Rev. B **22**, 359 (1980).

[36] J. G. Bednorz and K. A. Müller, Phys. Rev. Lett. **52**, 2289 (1984).

[37] S. Rod, Ph.D. thesis N. 927 (1991), Ecole Polytechnique Fédérale de Lausanne.

[38] H. Bilz, G. Benedek and A. Bussmann–Holder, Phys. Rev. B **35**, 4840 (1987); A. Bussmann–Holder, H. Bilz and G. Benedek, Phys. Rev. B, **39**, 9214 (1989).

[39] S. Rod, F. Borsa, J.J. van der Klink, Phys. Rev. B **38**, 2267 (1988).

[40] M. Fischer, A. Lahmar, M. Maglione, A. San Miguel, J. P. Itié, A. Polian and F. Baudelet, Phys. Rev. B **49**, 12451 (1994).

[41] H. Uwe, K. B. Lyons, H. L. Carter, P. A. Fleury, Phys. Rev. B **33**, 6436 (1986).

[42] H. Vogt, Phys. Rev. B **41**, 1184 (1990).

[43] K. Inoue, Jpn. J. Appl. Phys. **24**, Suppl. 24-2, 107 (1985).

[44] M. Maglione, S. Rod and U. T. Höchli, Europhys. Lett. 4 (5), 631 (1987).

[45] K. A. Müller, W. Berlinger, and E. Tosatti, Z. Phys. B – Condensed Matter **84**, 277 (1991).

[46] A. Okazaki, M. Kawaminami, Mater. Res. Bull. **8**, 545 (1973).

[47] W. N. Lawless, D. Rytz and U. T. Höchli, Ferroelectrics **38**, 899 (1981).

[48] Yasusada Yamada and Gen Shirane, J. Phys. Soc. Jpn. **26**, 396 (1969).

[49] J. D. Axe, J. Harada and G. Shirane, Phys. Rev. B **1**, 1277 (1970).

[50] O.-M. Nes, K. A. Müller, T. Suzuki, K. Fossheim, Europhys. Lett. **19**, 397 (1992).

[51] P. M. Gehring, H. Chou, S. M. Shapiro, J. A. Hriljac, D. H. Chen, J. Toulouse, D. Rytz, L. A. Boatner, Phys. Rev. B **46**, 5116 (1992).

[52] K. A. Müller, W. Berlinger and J. C. Slonczewski, Phys. Rev. Lett. **25**, 734 (1970).

[53] P. A. Fleury and J. M. Worlock, Phys. Rev. **174**, 613 (1968).

[54] V. Dvořák in: *Modern Trends in the Theory of Condensed Matter*. Proceedings of the XVI Karpacz Winter School of Theoretical Physics, 1979, Karpacz, Poland, ed. by A. Pçkalski and J. Przystawa, Lecture Notes in Physics; 115 (Springer-Verlag, 1980), p. 447.

[55] T. A. Aslanian and A. P. Levanyuk, Solid State Commun. **31**, 547 (1979).

[56] R. Martoňák, Magister PhilosophiæThesis, SISSA, Trieste, 1991.

[57] R. Oppermann, H. Thomas, Z. Phys. B **22**, 387 (1975).

[58] N. M. Plakida, A. Radosz and N. S. Tonchev, Phase Transit. **A29**, 179 (1991).

[59] R. Morf, T. Schneider and E. Stoll, Phys. Rev. B **16**, 462 (1977).

[60] T. Schneider and E. Stoll, Phys. Rev. Lett. **36**, 1501 (1976).

[61] M. Kolb, Phys. Rev. Lett. **51**, 1696 (1983).

[62] M. A. Moore, H. C. W. L. Williams, J. Phys. C: Solid St. Phys. **5**, 3168 (1972).

[63] M. A. Moore, H. C. W. L. Williams, J. Phys. C: Solid St. Phys. **5**, 3185 (1972).

[64] M. A. Moore, H. C. W. L. Williams, J. Phys. C: Solid St. Phys. **5**, 3222 (1972).

[65] P. Pfeuty, J. Phys. C: Solid St. Phys. **9**, 3993 (1976).

[66] M. Suzuki, Progr. Theor. Phys., **37**, 770 (1967).

[67] R. Martoňák, E. Tosatti, Phys. Rev. B **49**, 12596 (1994).

[68] J. C. Slater, J. Chem. Phys. **9**, 16 (1941).

[69] R. Martoňák, E. Tosatti, in preparation.

[70] R. Martoňák, E. Tosatti, in preparation.

[71] Yu. A. Freiman, V. V. Sumarokov, A. P. Brodyanskii, A. Jezowski, J. Phys.: Condens. Matter **3**, 3855 (1991).

[72] D. Marx, private communication.

[73] F. Moshary, N. H. Chen and I. F. Silvera, Phys. Rev. Lett. **71**, 3814 (1993).

FIGURE CAPTIONS

FIG. 1. The unit cell of a cubic perovskite ABO_3. When the central ion B is displaced towards an off-center position, the material becomes ferroelectric.

FIG. 2. A schematic picture showing the sudden appearance of the signal at 41.34 MHz in ^{181}Ta NMR in pure $KTaO_3$ [39]. The onset of the signal coincides with the would-be classical Curie temperature $T^* \simeq 40$ K, extrapolated from the high temperature part of the inverse dielectric constant curve (dashed line).

FIG. 3. A schematic picture showing the sudden enhancement of the Ti-O bond length fluctuations around temperature $T \simeq 30$ K, as measured by Ti K-edge EXAFS in $SrTiO_3$ [40]. This temperature is slightly lower than the would-be classical Curie-temperature $T^* \simeq 35$ K, extrapolated from the high temperature part of the inverse dielectric constant curve (dashed line).

FIG. 4. (a) Outer and inner Fe^{3+} fine-structure magnetic-field splittings with $\vec{H} \parallel [11\bar{2}]$ measured at a [111] stress of 1.97 kg/mm^2 in the $SrTiO_3$ tetragonal phase between 30 and 50 K due to the {001} domains. The middle splitting H_m^{tet} is due to {100} and {011} domains, which is not further discussed, but clearly shows the anomaly as well. (b) Outer $M = \pm 5/2 \leftrightarrow \pm 3/2$ and inner $M = \pm 3/2 \leftrightarrow \pm 1/2$ fine-structure magnetic resonance field differences with $\vec{H} \parallel [11\bar{2}]$ at a [111] stress of 31.4 kg/mm^2 in the trigonal phase. (After [45].)

FIG. 5. Phase diagram of [111] uniaxially p_{111} stressed $SrTiO_3$ as a function of temperature, showing the three-dimensional Potts line between the lower tetragonal and upper trigonal phases, and the dotted line T_q determined in both phases. (After [45].)

FIG. 6. Branches observed in $SrTiO_3$ at low q and ω by neutron scattering with $\vec{Q} = (\xi 02)$. The three highest branches are labeled TO for the A_{2u} mode, S for the E_g structural mode, and TA for the acoustic phonon. There is also an additional acoustic-like branch labeled A (filled symbols). (After [26]).

FIG. 7. Two different regimes of the quantum version of the standard single mode hamiltonian for structural phase transitions (4), depending on the relative importance of quantum fluctuations. (a) Weak tunneling regime. The ground state and first excited state energy levels are close to each other, and close to the bottom of the double-well potential. (b) Extreme quantum limit. The two lowest energy levels are well above the bottom of the well, and the gap between them is large with respect to the well depth.

FIG. 8. Phase diagram of the 2D Ising model in transverse field in the $(J/t, T/t)$ plane [65]. The solid line is the phase boundary between the disordered (para) region and the ordered (ferro) region. The dashed and dot-dashed lines are the crossover lines between the classical and quantum behaviour.

FIG. 9. Phase diagram of both unconstrained and constrained 2D quantum four-state clock model in the $(J/t, T/t)$ plane. Note the shift of the phase boundary towards lower J/t due to the constraint. (After [67]).

FIG. 10. The simplest concerted bond hopping mechanism, taking place on the elementary plaquette, around a closed loop.

FIG. 11. Mean-field zero-temperature phase diagram of the model with conserved bond vacancies in the $(J - V)$ plane. For simplicity, no ice-rule constraint has been applied. Apart from the usual ferroelectric phase with diagonal order, there is also a phase with ODLRO, for not too strong J and V.

FIG. 12. Origin of the effective quadrupolar interaction. If there is a B-O dipole bond $\vec{P}_i$ inside the cell i, the cell becomes elongated parallel to $\vec{P}_i$. The deformation propagates also to the neighbouring cells, where a dipole bond oriented along $\pm\vec{P}_i$ is favored.

FIG. 13. Mean-field phase diagram of the quantum four-state clock model with nearest-neighbour quadrupolar interaction in the $(J_Q/t, T/t)$ plane. Note the region of coupling J_Q, where the system re-enters from the ordered (Q) in the disordered (P) phase at low temperatures.

FIG. 14. Schematic mean-field zero-temperature phase diagram of the quantum four-state clock model with both quadrupolar and dipolar interaction in the (J, J_Q) plane. Note the existence of two ordered phases, one with quadrupolar order (Q) and one with dipolar order (usual ferroelectric phase). The dashed line corresponds to $J_Q/J = 3$.

FIG. 15. Schematic mean-field finite-temperature phase diagram of the quantum four-

state clock model with both quadrupolar and dipolar interaction in the (J,T) plane, for fixed ratio $J_Q/J = 3$. Decreasing temperature along the dashed line, passing close to the re-entrant area, we cross a region of enhanced quadrupolar fluctuations, without observing any particular feature on the static dielectric constant curve.

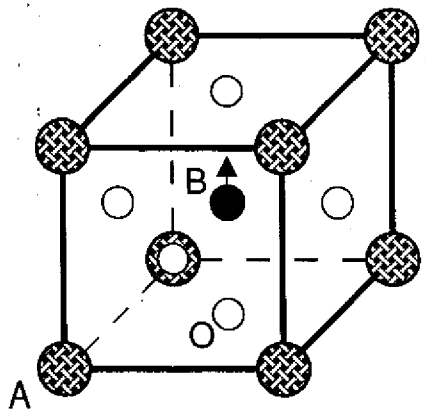

Fig. 1

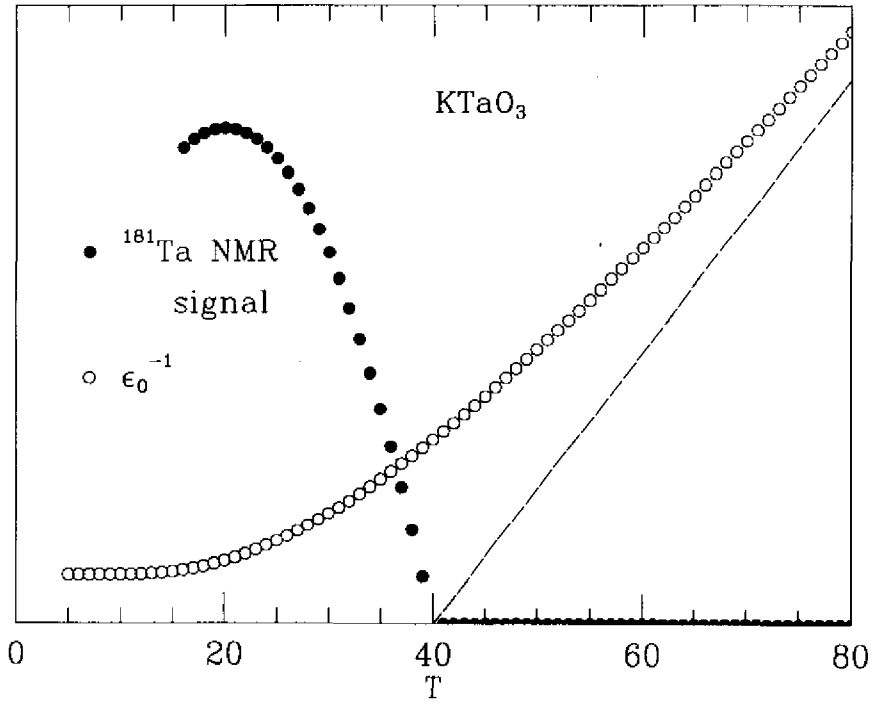

Fig. 2

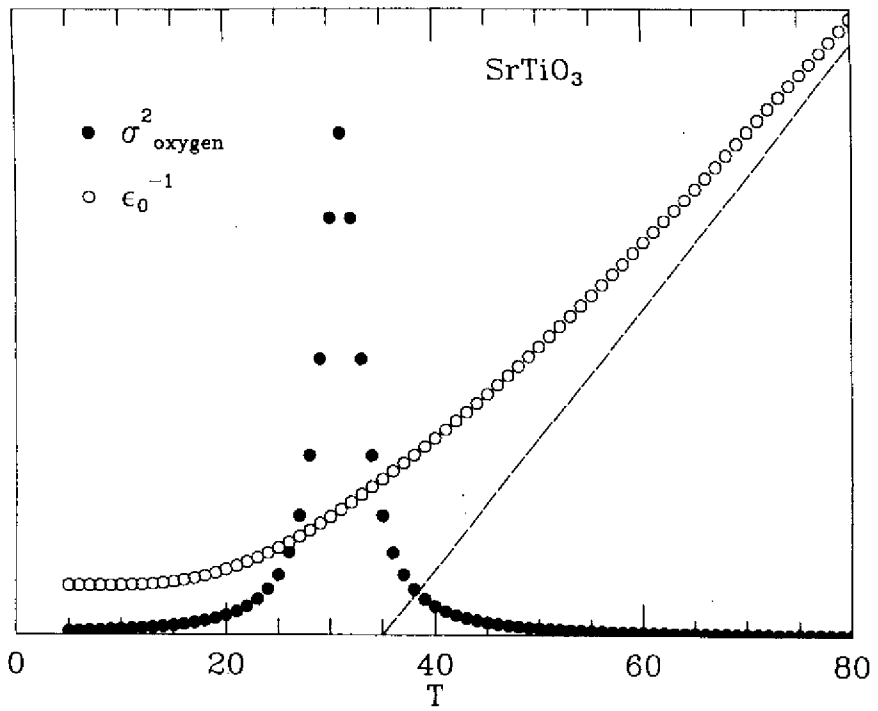

Fig. 3

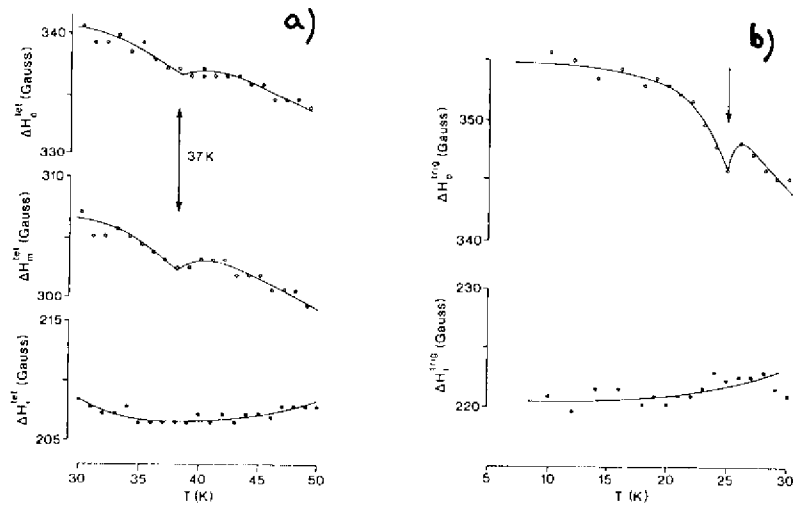

Fig. 4

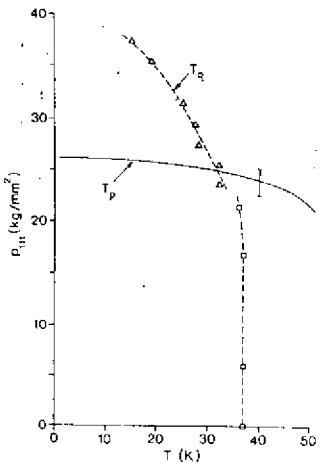

Fig. 5

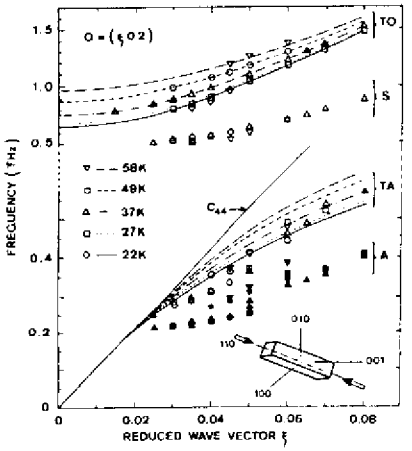

Fig. 6

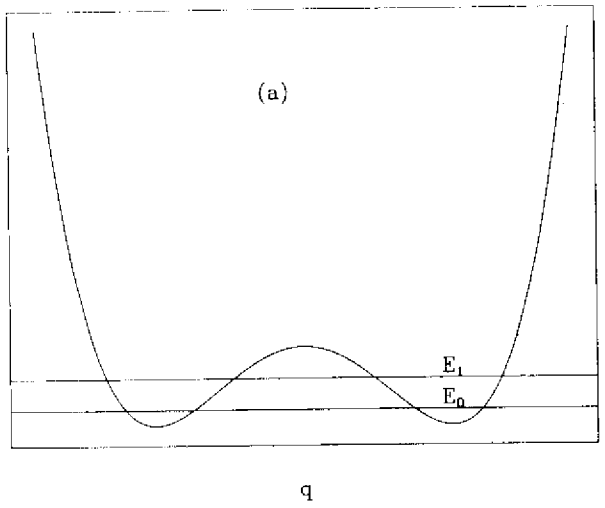

Fig. 7(a)

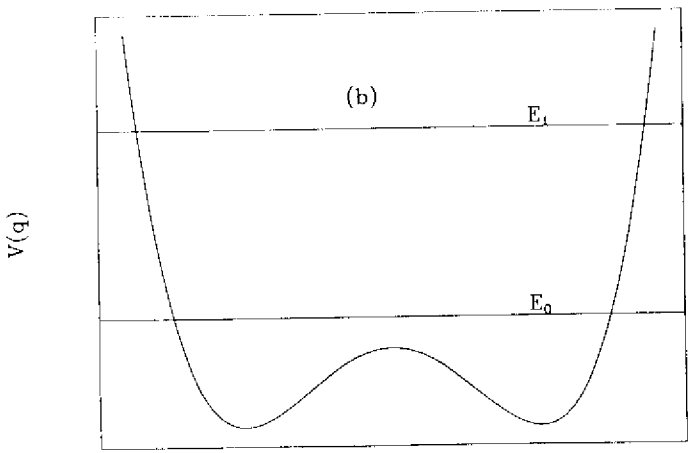

Fig. 7(b)

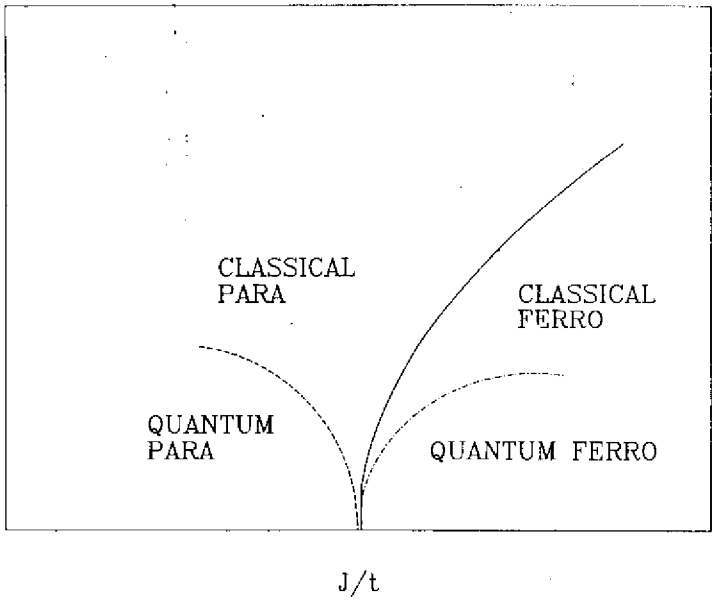

Fig. 8

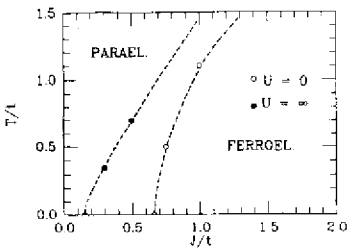

Fig. 9

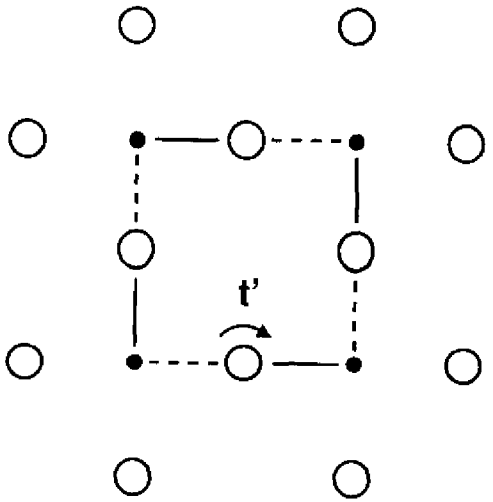

Fig. 10

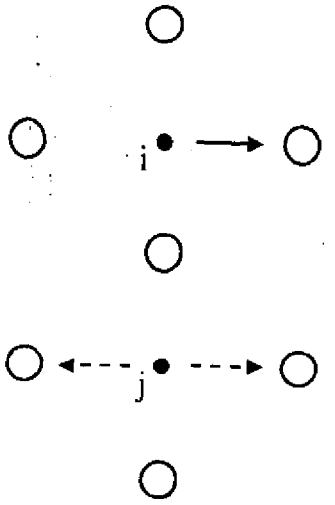

Fig. 12

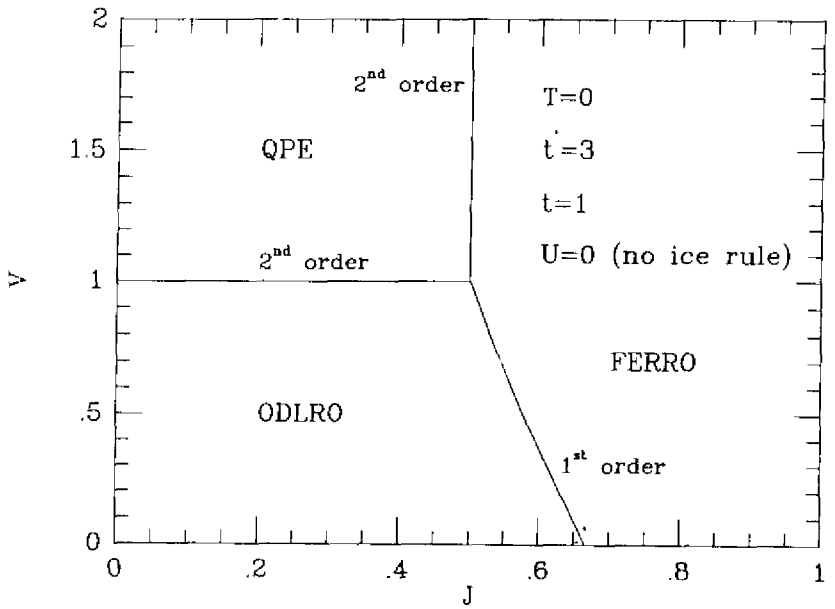

Fig. 11

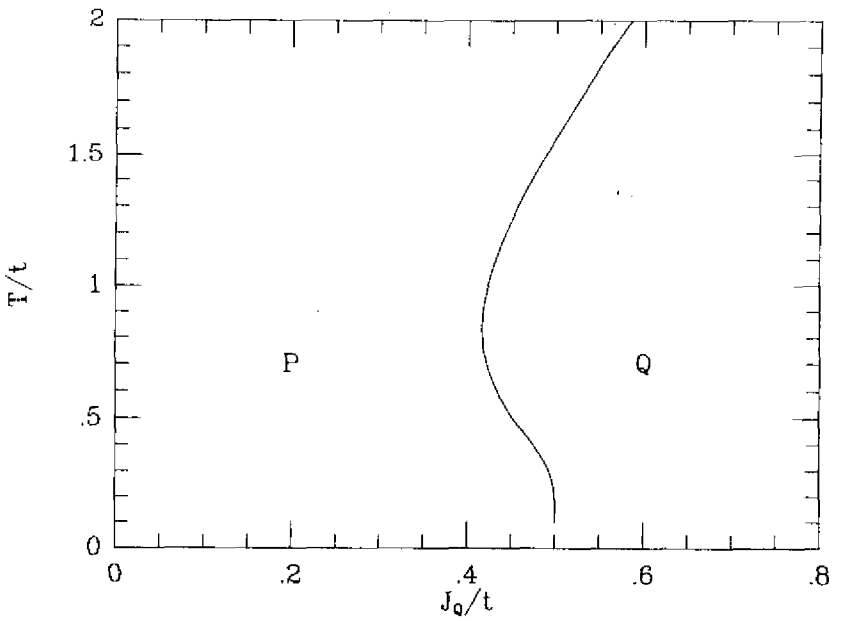

Fig. 13

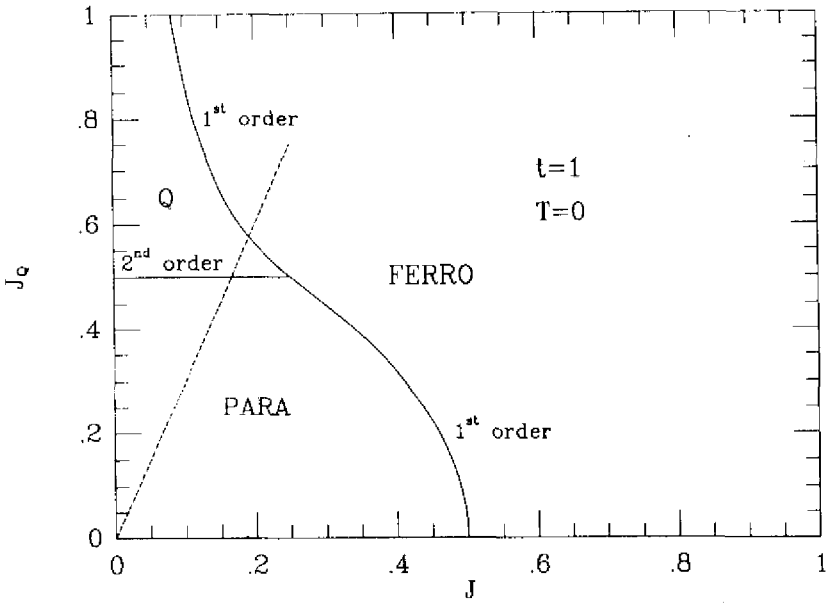
1
.8
.6
.4
.2
0
J_Q
1st order
Q
2nd order
t=1
T=0
FERRO
PARA
1st order
0
.2
.4
.6
.8
1
J

Fig. 14

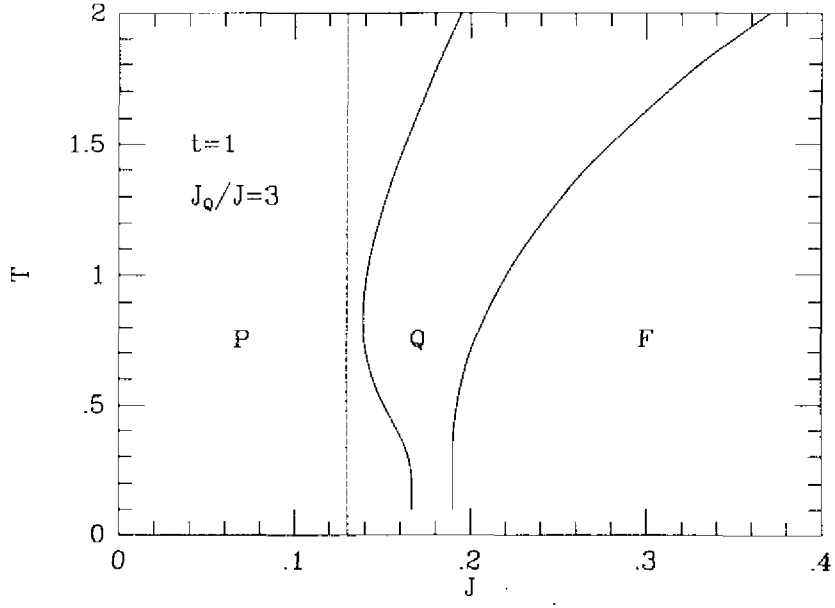
2
1.5
1
.5
0
T
t=1
$J_Q/J=3$
P
Q
F
0
.1
.2
.3
.4
J

Fig. 15